Applied Surface Science 436 (2018) 141–151

Contents lists available at ScienceDirect

Applied Surface Science

journal homepage: www.elsevier.com/locate/apsusc

Full Length Article

Use of micrometric latex beads to improve the porosity of hydroxyapatite obtained by chemical coprecipitation method

G.D. Webler[a], W.C. Rodrigues[b], A.E.S. Silva[c], A.O.S. Silva[d], E.J.S. Fonseca[e], M.F.S. Degenhardt[f], C.L.P. Oliveira[f], L. Otubo[g], D.A. Barros Filho[h,*]

[a] Instituto Federal de Alagoas (IFAL), Campus-Palmeira dos Índios, 57601-220, Brazil
[b] Instituto Federal de Alagoas (IFAL), Campus-Marechal Deodoro, 57160-000, Brazil
[c] Instituto Federal de Alagoas (IFAL), Campus-Maceió, 57020-600, Brazil
[d] Laboratório de Síntese de Catalisadores (LSCat), Centro de Tecnologia, Universidade Federalde Alagoas, Maceió, 57072-900, Brazil
[e] Grupo de Óptica e Nanoscopia (GON), Instituto de Física, Universidade Federal de Alagoas, Maceió, 57072-900, Brazil
[f] Instituto de Física, Universidade de São Paulo, Rua do Matão, 1371, CEP 05508-090, São Paulo, Brazil
[g] Laboratório de Microscopia e Microanálises (LMM), Instituto de Pesquisas Energéticas e Nucleares, IPEN-CNEN/SP, 05508-000, São Paulo, SP, Brazil
[h] Instituto Federal de Alagoas (IFAL), Campus-Maragogi, 57955-000, Brazil

ARTICLE INFO

Article history:
Received 21 July 2017
Received in revised form
11 November 2017
Accepted 26 November 2017
Available online 27 November 2017

Keywords:
Biomaterials
Composite materials
Surface properties
Chemical synthesis
Thermal properties
Latex beads

ABSTRACT

Hydroxyapatite is one of the most important biomaterials whose application mainly extends to implants and drug delivery. This work will discuss the changes in the pore size distribution of hydroxyapatite when there are latex beads present during the synthesis. These changes were monitored using different techniques: small angle X-ray scattering, X-ray diffraction, thermal gravimetrical analysis, N_2 adsorption, scanning and transmission electron microscopy. Latex beads and hydroxyapatite form a single nanocomposite with well-distinguished inorganic and organic phases. Latex bead removal in the temperature range of 300–600 °C did not modify the original crystalline structure of hydroxyapatite. However, the latex beads favored an increase in the adsorption capacity of mesopores at temperatures higher than their glassy transition (T_g). The main result of this research work consists on the increase of surface area and pore size distribution obtained after the removal of latex beads template. Latex beads have been used in a different approach changing the porosity of hydroxyapatite scaffolds not only introducing new routes for cell integration but also broadening the pore size distribution which can result in a more high efficiency for drug release in living cells.

1. Introduction

Hydroxyapatite [$Ca_{10}(PO_4)_6(OH)_2$] is one of the most important biomaterials because it is the main inorganic component of bones and teeth. Its biocompatibility and osteoconductivity properties has become notably attractive for implant materials and drug delivery systems [1,2]. There are two methods to synthesize hydroxyapatite: solid-state and wet methods. The first method is based on a high sintering temperature, at which the inorganic precursors are mixed to form hydroxyapatite Different techniques can be apllied to change hydroxyapatite particles properties synthesized by wet chemical method.

An advantage of this method is the production of samples with a homogeneous composition, which can be processed into coatings on usual implant materials such as alumina [3] and titanium [4]. Coprecipitation is based on the combination of an inorganic precursor such as calcium nitrate [$Ca(NO_3)_2$] and ammonium phosphate monobasic ($NH_4H_2PO_4$), which acts as a phosphate ion source. These two reagents form an aqueous solution, which is maintained at a basic pH by the addition of ammonium hydroxide (NH_4OH).

The synthesis conditions of wet chemical method can play a vital role to generate hydroxyapatite with different morphologies. Li-yun et al. [5] reports that it is possible to obtain hydroxyapatite particles with the aid of ultrasonic irradiation using $Ca(NO_3)_2$ and $NH_4H_2PO_4$ as source material. They observed that spherical nanoparticles could be obtained at high synthetic temperature (353 K), ultrasonic power (300 W) and high Ca/P ratio (2.0–2.5). Other conclusion is that synthetic conditions like [Ca^{2+}] concen-

* Corresponding author.
E-mail addresses: geovana_dw@hotmail.com (G.D. Webler), wagnercirilorodrigues@gmail.com (W.C. Rodrigues), antonyessilva@gmail.com (A.E.S. Silva), osimar@yahoo.com (A.O.S. Silva), eduardo@fis.ufal.br (E.J.S. Fonseca), mfs@if.usp.br (M.F.S. Degenhardt), crislpo@if.usp.br (C.L.P. Oliveira), lotubo@gmail.com (L. Otubo), djalneno@gmail.com, djalma.filho@ifal.edu.br (D.A. Barros Filho).

https://doi.org/10.1016/j.apsusc.2017.11.218
0169-4332/

tration and synthetic temperature and ultrasonic power change the crystallite size of hydroxyapatite particles. It is also possible to change mechanical properties of hydroxyapatite after wet chemical synthetic procedure. This feature has been highlighted by Wei et al. [6] who produce high-quality crack-free coatings using rounded particles obtained by precipitation of calcium phosphate and subsequent alkali digestion in aqueous ammonia at a pH of 11–12. They applied electrophoretic deposition as a post-synthesis procedure and coated Ti6Al4V substrate with different hydroxyapatite precipitates. It has been concluded that cracking susceptibility is correlated with the particle shape in such a way that round particles due to their equi-axed geometry can generate free crack coatings by electrophoresis technique.

The wet method results in hydroxyapatite samples whose surface morphology has a random distribution of particles with different sizes, which depend on the pH and temperature of the solution. Some attempts have been reported in the literature to change the hydroxyapatite morphology, which is mainly restricted to beads or rods. This goal is possible using surfactants such as cetyltrimethylammonium bromide (CTABr) [7], sodium dodecyl sulfate (SDS) [8] and triblock copolymer (F-127) [9]. Zhao et al. reported that it is possible to obtain either spherical or rod-like hydroxyapatite particles by changing only the surfactant concentration [10]. In this work, it is also observed that spherical hydroxyapatite has a bimodal distribution of pores centered at 2.5 nm and 3.0 nm.

Nanoparticles have been used as templates for crystallization of hydroxyapatite through the generation of organic/inorganic hybrid materials. This biomimetic approach is based on encapsulation of preformed inorganic materials within a polymeric matrix as it has been highlighted by Ethirajan et al. [11]. The syntethic route is based on the monodispersity and large surface area of poly(styrene-*co*-acrylic acid) latex particles with diameters below 500 nm. It was used covalently functionalized particles bound to carboxyl groups on their surface to perform crystallization of hydroxyapatite. The functionalization of these particles happened at pH 10 by carboxyl groups resulting on the attachment of Ca^{2+} and PO_4^{3-} ions and posterior coverage of the polymeric surface. Crystallite size was estimated through (002) reflection in the range from 19 to 22 nm. It has been concluded that the crystallite size was the same on the particle or in the solution. The growth of hydroxyapatite using nanoparticles templates has been attractive in terms of fabrication of scaffolds for osteointegration and bonding between the implant and the bone. This feature is associated mainly to the potential of using the polymeric nanoparticles for drug release and wound healing promotion in an efficient way than usually observed in scaffolds prepared without organic template [12,13].

In recent years, particular attention has been paid to the preparation of Hydroxyapatite bioceramics with porous morphology, which are notably interesting for bone regeneration because they mimic natural bone in terms of chemical composition and microstructure [14–16]. The porosity in a biomaterial implant allows ingrowth and regeneration of natural bone. It is worth mentioning that the increase in surface area, which results from the porosity, also contributes to a delivery agent capacity to adsorb a drug [1]. Several processes are currently used to produce porous ceramics. The simplest technique is based on incorporating the organic phase in the ceramic material composition, in controlled proportions and sizes, which leaves voids with the same size of the organic phase materials after the disposal [17]. Other more elaborate methods, such as aerogel [18], hydrogel [19,20] and bio-organics [21,22], can generate a structure with nanometer-sized pores.

Latex beads can be considered a suitable choice to obtain porous hydroxyapatite because they can be easily removed using chemical etch or heat treatment, where large pores are connected and surrounded by thin walls of an inorganic phase. There are few reports about the application of porous hydroxyapatite templated by latex beads. It has been used poly(ϵ-caprolactone) (PCL) microspheres to produce porous hydroxyapatite applied as scaffolds in tissue engineering and sustained release of therapeutics [23]. Hydroxyapatite nanoparticles stabilized the dispersion of emulsions and microspheres whose diameter is in the range of 9.2–25.1 μm. The use of huge polystyrene spheres ($\phi > 70\,\mu m$) as three dimensional template for hydroxyapatite scaffolds have been described by Kotov et al. [24]. They introduce the use of inverted colloidal crystals as three dimensional cell support and they conclude that human hepatocellular carcinoma HEP G2 form a large number of 10–15 cell colonies on scaffolds made from 75 μm spheres and human bone marrow HS-5 cell cultures generate smaller colonies consisting of three to four cells in 90 μm cavities. Therefore, size scale of latex beads can determine the bioactivity of hydroxyapatite, however porous hydroxyapatite templated by latex beads in micrometric range ($\phi < 10\,\mu m$) is still unknown. Only Fujishima et al. [2] reported that it is possible to incorporate hydroxyapatite in latex beads assembled using the gravity sedimentation method. They observed that small latex beads ($\phi \sim 200$ nm) form a hierarchical trimodal porous hydroxyapatite structure at 330 °C. However, it is very hard to obtain self assembled films of latex beads in the micrometric range (>1,000 nm) due to effect of gravity or thermal agitation during the formation of colloidal template.

These approaches to obtain porous hydroxyapatite are necessary because they can be applied in two importantant fields of biomaterial research: tissue engineering and drug delivery. The application of porous hydroxyapatite in tissue engineering is related to the following properties of this material like biocompatibility, osteoconductivity, interconnected porous structure, appropriate mechanical strength, and biodegradability. Scaffold can induce not only the formation of new bone but also it can act as a carrier or template for implanted bone cells or other agents [25,26]. This feature highlights how is important to have an interconnected porous structure for the introduction of bone cells, osteotropic agents, or vasculature into the pores. It has been reported that weak interconnection of the pores can play a vital role for bone regeneration because it can avoid their replacement for new bone tissues [27]. It is possible to create new pores networks for hydroxyapatite ceramics (IP-CHA) as it has been described by Yoshikawa et al. [28]. In this work, it has been mixed IP-CHA in combination with bone morphogenetic protein (BMP), mesenchymal stem cells from bone marrow, and vascular prefabrication to improve tissue regeneration allowing the introduction of bone cells, osteotropic agents, or vasculature into the pores. There are many other works about the generation of hydroxyapatite with micro-sized structure, however, there is an increasing interesting in nanosized hydroxyapatite because they have the same morphology of mineral crystals found in bone [29,30]. Therefore, they are good candidates to enhance the mechanical properties of implants and their osteoconductivity. Other feature to be highlighted is their ability to enhance osteoblast adhesion by control protein interactions in terms of adsorption, configuration, and bioactivity due to their higher surface to volume ratio.

Hydroxyapatite scaffolds can be considered as potential substrate for drug delivery system because they incorporate drugs retaining in a specific target site and deliver it gradually in the diseased cells. They have been used for release of antibiotics anti-inflammatory, analgesic and anticancer drugs as it has been reported by Ginebra et al. [31]. Drugs delivery systems have been improved using hydroxyapatite due to its bioactivity, however, there is lost of the biofunctionality when there is the incorporation of therapeutic agents. Polymers have been used to remain the mechanical stability and to improve tissue interaction of scaffold and bone tissue due to their biodegradable and

easy-processing characteristics [32–35]. There are many reports about the preparation of hydroxyapatite polymers nanocomposites like Hydroxyapatite/chitosan, Hydroxyapatite/polyurethane, Hydroxyapatite/poly(lactic acid), and Hydroxyapatite/poly(lactic-*co*-glycolic acid) (PLGA) which can be used as drug delivery systems [36]. Polymeric microspheres are suitable choices to deliver cytokines and proteins [37,38] with interesting properties like biodegrability in the human body and plasticity in fabrication. The drug release kinetics can be controlled by microsphere because their degradation rate can be determined by the composition of monomer units and by the microsphere size and morphology [39–41]. However, hydroxyapatite scaffolds have huge pores (>100 μm) and microspheres are very small compared to their dimensions (<10 μm). It is expected that there is decrease of their mechanical properties in terms of compressive strength and elastic modulus of this kind of scaffold. One possibility is to decrease the pore size of latex bead and to introduce interconnected pores inside the scaffolds by mixing latex bead into hydroxyapatite matrix during its synthesis.

In the present study, micrometric latex beads (1.3 μm) were incorporated into hydroxyapatite during synthesis using the wet method and were removed using a heat treatment. This approach allows the investigation on how latex beads interact with Hydroxyapatite and form huge aggregates (in micrometric scale), and also the coverage of latex surface by Ca^{2+} and HPO_4^{2-} ions. The samples were characterized using small angle X-ray scattering (SAXS), X-ray diffraction (XRD), thermal gravimetrical analysis (TGA), N_2 adsorption, scanning and transmission electron microscopy (SEM and TEM). Ours findings showed that it was possible to prepare porous hydroxyapatite incorporated into a micrometric latex bead network and to remove the beads while maintaining the original pore architecture, which was notably similar to that found in hard tissues such as bone and teeth. This procedure maintained the microstructure of the nanocomposite and resulted in a porous hydroxyapatite with no changes in the crystalline structure, as comproved by SAXS and XRD. However, there is an increase in surface area, which is associated with the new porous architecture that was induced by the introduced latex beads inside the hydroxyapatite bulk during the synthesis process.

2. Materials and methods

Hydroxyapatite was synthesized according to the chemical wet method based on the following reaction:

$$10Ca(NO_3)_2.4H_2O + 6NH_4H_2PO_4 + 14NH_4OH \rightarrow$$
$$Ca_{10}(PO_4)_6(OH)_2 + 20NH_4NO_3 + 52H_2O$$

It has been used 0.072 mols of calcium nitrate ($Ca(NO_3)_2$ – Sigma Aldrich) and 0.030 mols of ammonium phosphate monobasic ($NH_4H_2PO_4$ – Sigma Aldrich). Calcium nitrate has been dissolved at water (~100 mL) and mixed 50 mL polystyrene latex aqueous dispersion (Invitrogen-mean diameter: 1.3 μm). This mixture was added drop-wise into a solution of ammonium phosphate monobasic ($NH_4H_2PO_4$ – Sigma Aldrich), which was maintained at ambient temperature under constant stirring (300 RPM). NH_4OH was used to adjust the solution to raise the pH of the 10.4 in order to obtain a stoichiometric ratio Ca/P = 1.67. The final product was a white powder with 5 g weight after drying at 100 °C.

Subsequently, the mixture was stirred for 1 h, and the precipitate was aged for 50 h, washed, filtered, and dried in a stove at 100 °C for 24 h. This sample is labeled T_0. Five samples were heat-treated at 200, 300, 400, 500 and 600 °C for 1 h in a tubular oven (EDG, model FT-HI/40) at a heat rate of 1 °C min^{-1}.

The thermal behavior (TG/DTA) analysis of raw materials were performed using a Shimadzu DTG-60H in the temperature range of 25–800 °C with a heating rate of 1 °C min^{-1} in a dynamic atmosphere of nitrogen (50 mL min^{-1}).

The characteristic functional groups present in the prepared materials were assessed on an infrared spectrometer (IR) (Prestige-21) equipped with a diffuse reflectance accessory (DRS-8000). For sample preparation, the powder sample (1 mg) was mixed with a non-absorbing standard (KBr, 100 mg) on a holder. The IR spectra were recorded in the 4000 to 500 cm^{-1} region.

The X-ray diffraction (XRD) pattern was obtained with Cu K-alpha radiation (0.15418 nm), using a scintillation counter and a graphite [002] bent monochromator in a Rigaku 3 kW generator and an Ultima III model theta-theta camera. The X-ray tube was set to 40 kV/30 mA. The measurements, in a Bragg–Brentano theta-2 theta geometry, was performed with step scanning of 0.05° and counting time of 7 s/step. A total angular 2 theta range from 10° to 60° was collected. The crystal size (D_{hkl}) was calculated from the XRD line-broadening measurements based on Scherrer equation:

$$D_{hkl} = 0.89 * \lambda/(\beta * \cos\theta_{hkl}) \quad (1)$$

where λ is the X-ray wavelength, β is the line broadening at half the maximum of the Hydroxyapatite (002) line, and $\theta_{(hkl)}$ is the peak diffraction angle for the (*hkl*) plane. The shape factor k is usually taken as about 0.89 for spherical shape [42]. In this work, hydroxyapatite particles were considered approximately spherical.

SAXS measurements were performed on the XEUSS-Xenocs equipment, placed at the Institute of Physics, University of São Paulo. The powder samples were placed on a sample holder between Kapton slides. SAXS measurements were performed simultaneously using two area detectors. Background measurements were made under the same conditions, allowing subtracting from the experimental data the unwanted scattering. Scattering data were modeled by Indirect Fourier Transform (IFT) method [43], which provides the volume distribution function DV(r) and average gyration radius (R_G).

Scanning electron microscopy (SEM) was performed using a Shimadzu Super scan SSX-550 microscope to determine how the presence of the latex beads changed the topography of the hydroxyapatite samples. The SEM measurements were performed after the gold metallization of the samples.

Transmission electron microscopies (TEM) were obtained using a Jeol JEM-2100, operating at 200 kV. The powder samples were suspended in isopropanol by sonication. A drop of the sample suspension was placed on copper grid coated with colloid film and allowed to dry before TEM analysis.

The surface area and the mean pore size were determined based on the nitrogen adsorption-desorption isotherms at liquid N_2 temperature on a Micrometrics (ASAP 2010) instrument. The specific surface area was determined using Brunauer–Emmett–Teller (BET) method. The mean pore size was estimated from the desorption branch of the nitrogen adsorption-desorption isotherms using Barrett–Joyner–Halenda (BJH) method [44–46].

3. Results and discussion

Fig. 1A and B show the TG/DTA curves for hydroxyapatite without and with latex beads. It is observed that the latex beads modify the thermal behavior of hydroxyapatite and introduce four regions for mass losses. Region I occurs in the range of 30–120 °C, which is attributed to the water removal from the hydroxyapatite surface. The second event of mass loss (Region II −120 °C < T < 275 °C) is ascribed to the desorption of water and other volatile compounds that were trapped between the latex beads and the surface of the hydroxyapatite particles and pores. Region III is attributed to the

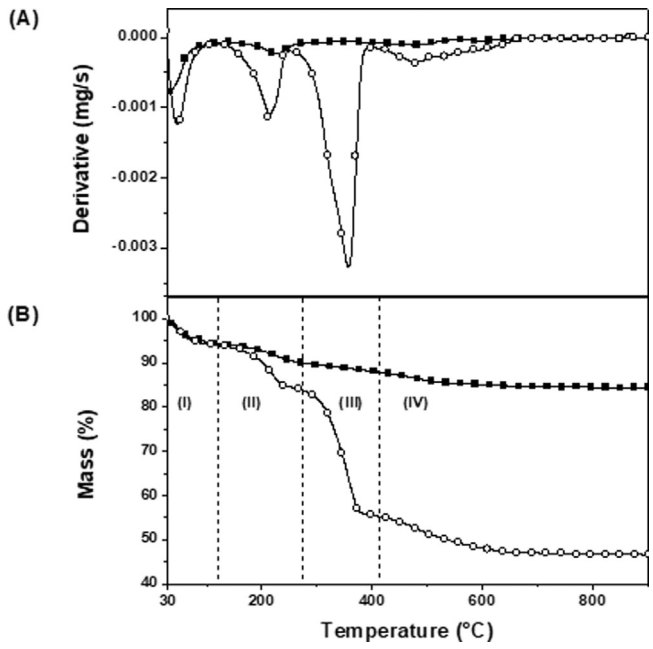

Fig. 1. Thermal behaviors of Hydroxyapatite (■) and Hydroxyapatite + Latex beads (○): (A) – DTG; (B) – TG. The meaning of the four regions I–IV is discussed in the text.

thermal degradation of the latex beads and outlet gas components from other thermal cracking and decomposition reactions of the polymer that extends over the range from 275 °C < T < 410 °C. The mass losses are more prominent for hydroxyapatite mixed with latex beads because they constitute more than 40% of the weight sample. This result was obtained considering that water is mainly trapped to hydroxyapatite sites and the sample is completely dried before TGA characterization. Region IV (T > 410 °C) is attributed to the slow oxidation of carbonaceous residues, which results from the thermal degradation of the latex beads.

Fig. 2 shows Fourier Transform infrared (FTIR) for three hydroxyapatite samples. It can be seen the broad transmission peak of phosphate stretching mode at 960, 1040 and 1090 cm^{-1}. There is also the O—H vibration mode at 634 and 3557 cm^{-1}. According to Fujishima et al. [2], this is characteristic of a rigid crystalline structure through high temperature calcination. It can also be observed that there is a reduction of the transmittance band of carbonate ions at 1410 and 1510 cm^{-1} due to their substitution by phosphate ions. The double bond stretching C≈C appears at 1647 cm^{-1}. There is a broad band at 3200–3500 cm^{-1} related to the presence of a hydroxyl group, generated after the hydrolytic ring opening of epoxy group as it has been observed by Aielo et al. [47] for natural rubber latex membranes. FTIR characterization displays the absence of hazard biological compounds after heat treatment at 600 °C/1 h. This trend is important for future application of hydroxyapatite as a biomaterial for tissue engineering or drug delivery.

Fig. 3 shows the morphological features of hydroxyapatite mixed with latex beads. It is observed that latex beads are soaked in hydroxyapatite at 100 °C and 200 °C (Fig. 3A and B). There are two distinct phases in the sample without any visible interaction between latex beads and hydroxyapatite. At 300 °C, the latex beads appear bound in the bulk of the sample, as indicated by the white arrows (Fig. 3C). The latex beads begin to be removed at 400 °C, as indicated by the spherical shells along the surface sample (Fig. 3D). At 400 °C, the latex beads melt, completely covering the hydroxyapatite and forming a single nanocomposite. The porous network is formed in the temperature range of 500–600 °C (Fig. 3E and F). The pores are randomly distributed along the external surface of the samples, and their estimated diameters are below 1 μm.

Fig. 4 shows TEM images for samples dried at 100 °C and 200 °C/1 h. It can be seen that there is a mixture of latex bead and Hydroxyapatite (Fig. 4A and B). Both samples have rod particles with variable size smaller than 50 nm (Fig. 4C and D). High resolution TEM images show some regions with crystalline planes (Fig. 4E and F) for these samples. Fig. 5 displays TEM images for samples calcined at 300 °C/1 h and 400 °C/1 h. It is observed that the hydroxyapatite particles are embedded in amorphous material for sample calcined at 300 °C/1h (Fig. 5A). The surface is more dense and isolated particles cannot be distinguished for the sample calcined at 300 °C/1 h (Fig. 5C and E). This trend can be associated to early melting/decomposition of the latex beads. This effect is not so intense for sample calcined at 400 °C/1 h. It can be seen that spherical shells begin to be formed (Fig. 5B) and there are gray regions where hydroxyapatite is less dense forming a small coating along the latex bead surface (Fig. 5D). The hydroxyapatite particles seem to be very small (<50 nm) and embedded in a thin layer of organic

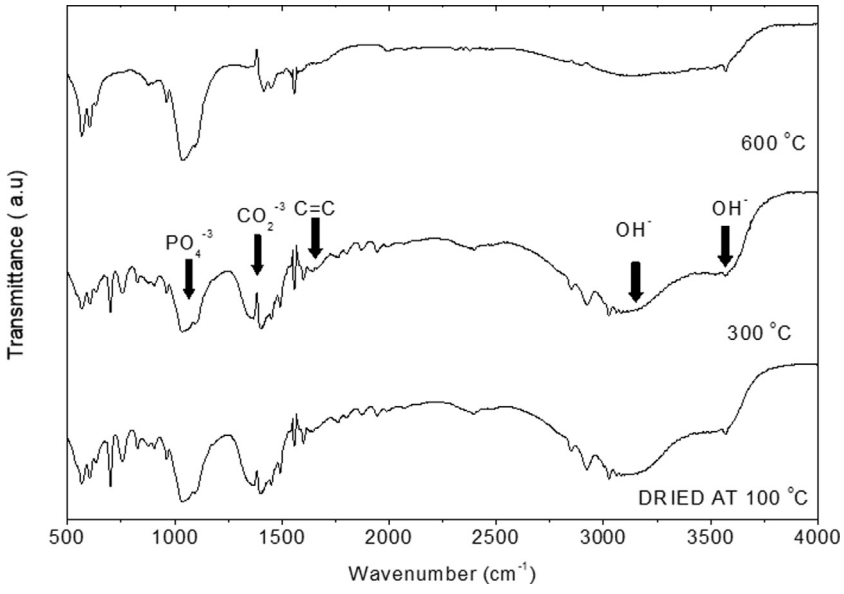

Fig. 2. FTIR spectra of three samples: dried at air; heat treated at 300 °C/1 h; heat treated at 600 °C/1 h. The transmittance bands are explained in the text.

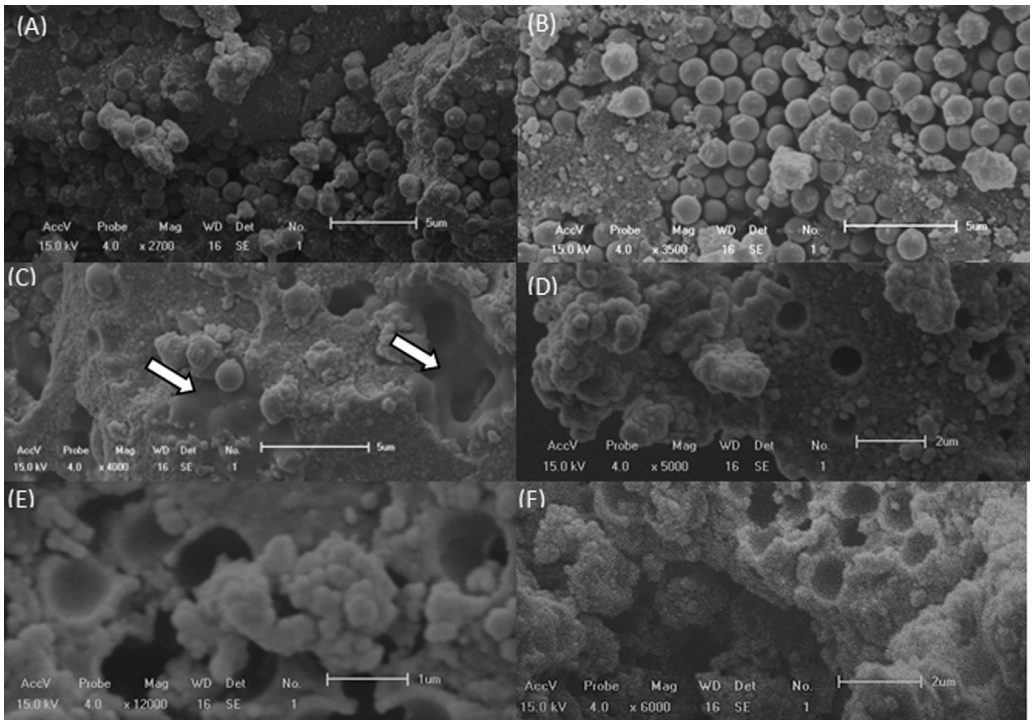

Fig. 3. Scanning electron microscopy images of hydroxyapatite mixed with latex beads and calcined at different temperatures: (A) – Dried at 100 °C; (B) – 200 °C/1 h; (C) – 300 °C/1 h; (D) – 400 °C/1 h; (E) – 500 °C/1 h; (F) – 600 °C/1 h. The white arrows indicate the changes of the latex beads in the bulk of the hydroxyapatite sample, which was treated at 300 °C.

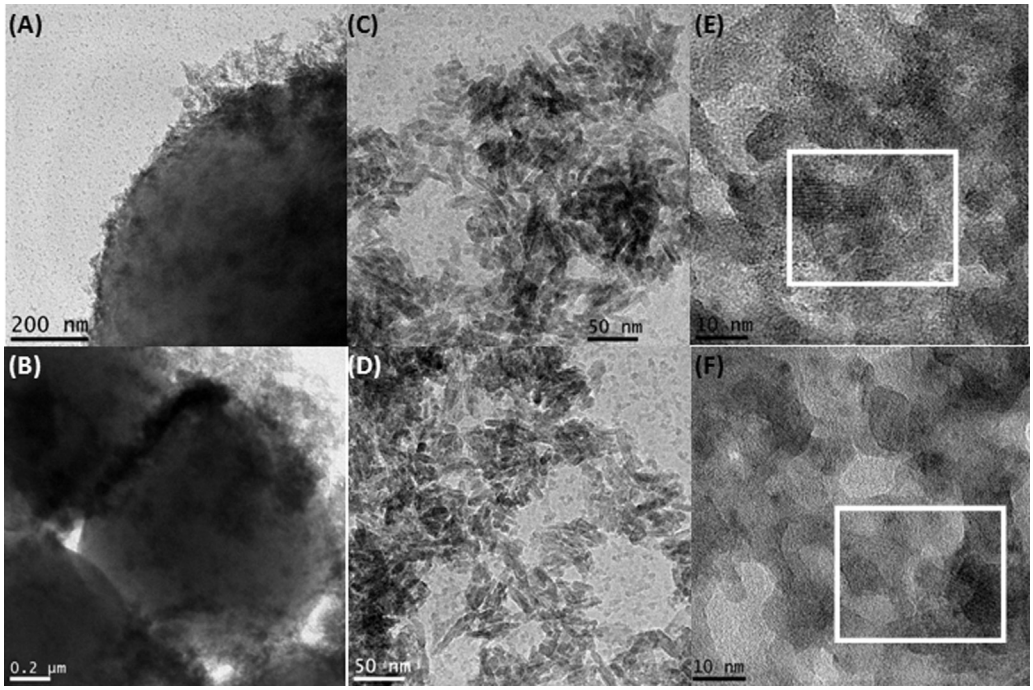

Fig. 4. Transmission electron microscopy images of hydroxyapatite mixed with latex beads after drying at 100 °C and calcinating at 200 °C/1 h: (A) – coverage of latex beads by hydroxyapatite (100 °C); (B) – coverage of latex beads by hydroxyapatite (200 °C/1 h); (C) – hydroxyapatite particles in rod shape (100 °C); (D) – hydroxyapatite particles in rod shape (200 °C/1 h); (E) – crystallographic planes of hydroxyapatite displayed by white square (100 °C); (F) – crystallographic planes of hydroxyapatite displayed by white square (200 °C/1 h).

material generated by the residue of the melting of latex beads (Fig.5F). Fig. 6 shows TEM images for samples calcined at 500 °C/1 h and 600 °C/1 h. There is the formation of macroporous network due to the absence of latex beads that were soaked in hydroxyapatite matrix (Fig. 6A and B). It can be seen that macropores have the same size of latex beads (Fig. 6C and D). The walls of these fragments are constituted by aggregated hydroxyapatite particles as it can be seen at Fig. 6E and F. These walls are different in relation

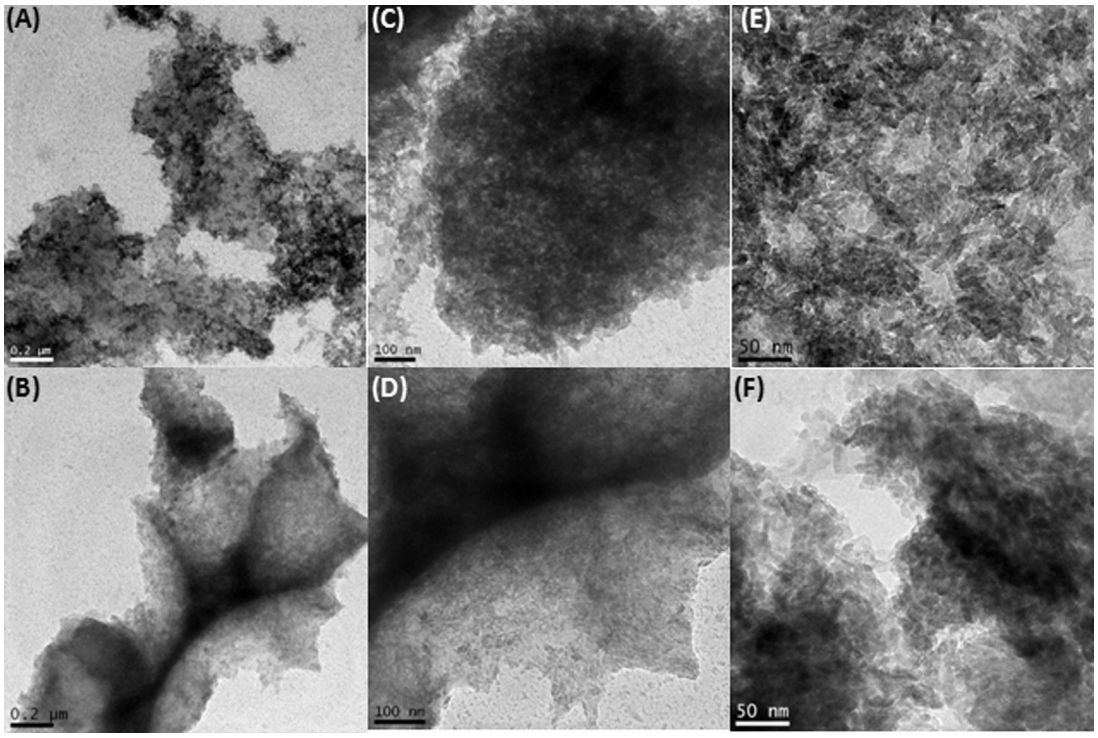

Fig. 5. Transmission electron microscopy images of hydroxyapatite mixed with latex beads after calcination at 300 °C/1 h and 400 °C/1 h: (A) – densification of latex beads covering hydroxyapatite particles (300 °C/1 h); (B) – spherical shells caused by remotion of latex beads (400 °C/1 h); (C) – hydroxyapatite surface covered by organic material (300 °C/1 h); (D) – boundary of two macropores generated by remotion of latex beads (400 °C/1 h); (E) – compact surface of hydroxyapatite clusters (300 °C/1 h); (F) – compact surface of hydroxyapatite clusters (400 °C/1 h).

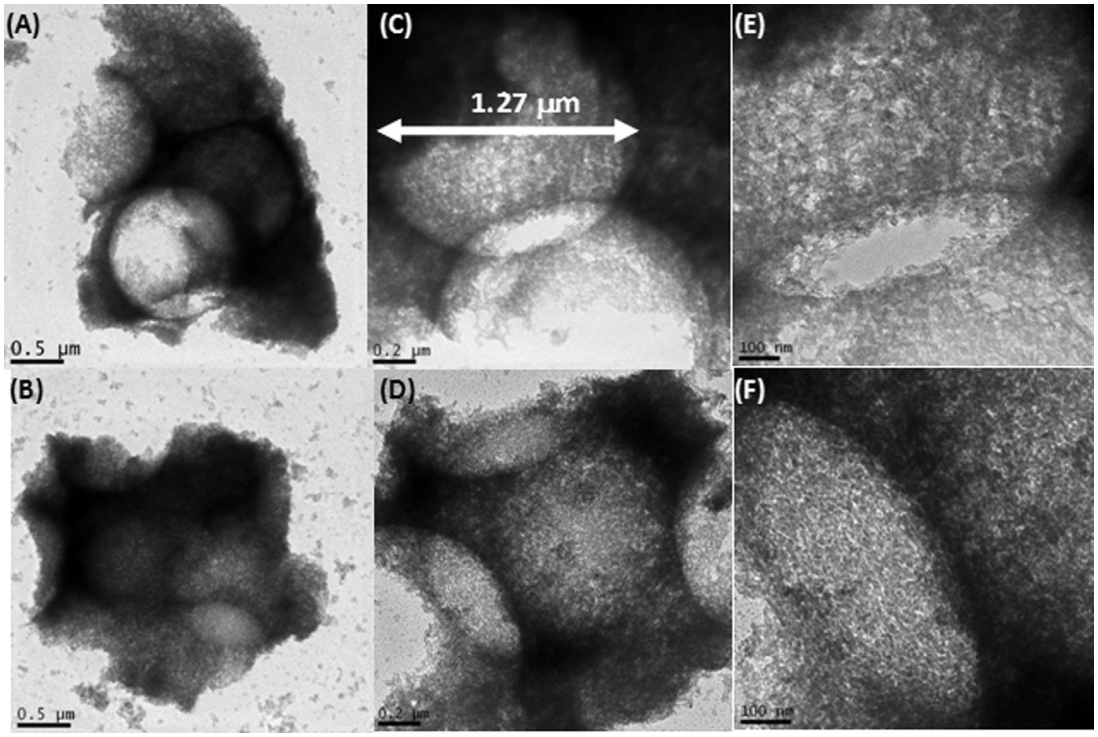

Fig. 6. Transmission electron microscopy images of hydroxyapatite mixed with latex beads after calcination at 500 °C/1 h and 600 °C/1 h: (A) – huge macroporous generated by remotion of latex beads (500 °C/1 h); (B) – huge macroporous generated by removal of latex beads (600 °C/1 h); (C) – detailed view of hydroxyapatite spherical shell (500 °C/1 h); (D) – detailed view of hydroxyapatite spherical shell (600 °C/1 h); (E) – boundary of two macropores generated by remotion of latex beads (500 °C/1 h);(F) – boundary of two macropores generated by remotion of latex beads (600 °C/1 h).

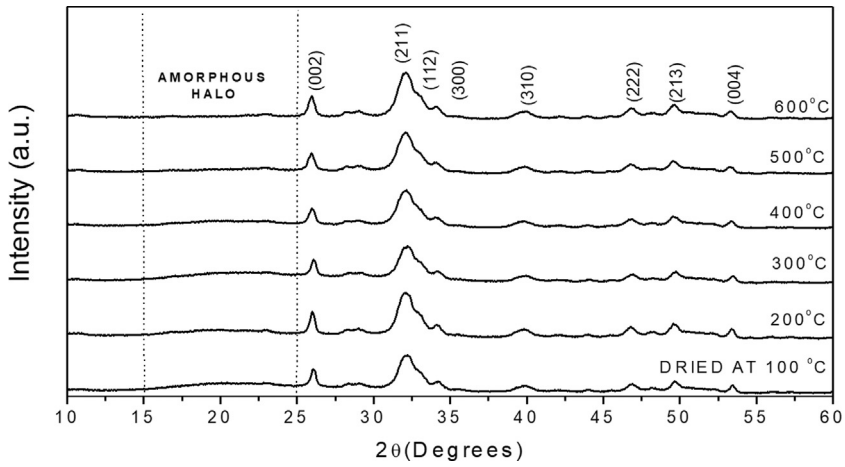

Fig. 7. X-ray diffraction patterns of hydroxyapatite mixed with latex beads and calcined at different temperatures. Miller indexes of the peaks were indexed according to the letter 89-6438 [48].

Table 1
Crystal size, surface area, and radius of gyration for hydroxyapatite mixed with latex beads. The crystallite size was determined by 002 line.

Treatment Temperature (°C/1 h)	Crystal Size (nm)	Surface Area (m^2/g)	Radius of Gyration (nm)
100	16.86	108.25	17.81
200	17.30	65.86	17.71
300	17.56	48.74	16.61
400	17.43	0.20	14.32
500	21.44	73.16	14.58
600	17.48	211.03	11.76

to the sample treated at 400 °C/1 h because there is not a thin film between hydroxyapatite particles generated by decomposition of latex beads.

Fig. 7 shows the XRD diffractograms of the samples that were treated at different temperatures. Each pattern shows hydroxyapatite as the only crystalline phase. The crystallographic plans were allocated on the basis of letter 89-6438 [48]. The broad peak at approximately 2θ = 32° is ascribed to an overlapped peak of the (211), (112), and (300) reflections of hydroxyapatite, and this peak broadening is attributed to the small crystalline size and low crystallinity of the Hap nanoparticles. It is clearly observed that there is amorphous halo in 2θ between 25 and 28°. This halo begins to change from the sample at 400 °C and at 500 °C. Interestingly, for 600 °C there is a recovery of the peak high. For samples between 300 °C and 600 °C peaks corresponding to (002) and (310) reflections are greatly attenuated while the peaks (211), (112), and (300) reflections remain.

Table 1 displays the crystal size of hydroxyapatite with the increase in heat treatment temperature. These results have been obtained by XRD characterization and calculated using Eq. (1). The latex beads do not significantly change the crystal growth, which it is not expected in the absence of latex beads. Studies show that with the increase in calcination temperature, the grain size of the Hydroxyapatite nanoparticles increases [49]. The R_G values decrease at higher calcination temperatures indicating that there is the formation of isolated scattering centers.

The isotherm adsorption curves for hydroxyapatite samples are shown in Fig. 8. In all cases, the isotherm curves have identical behaviors and can be classified as Type IV with loop H3 [45,46]. Type-IV isotherm has a limiting uptake over a range of high P/P_o, and its hysteresis loop can be associated with the capillary condensation in mesopores. These isotherm curves also have an H3 loop, which can be associated to slit-shaped pores because of the presence of aggregates such as plate particles. It can be seen that

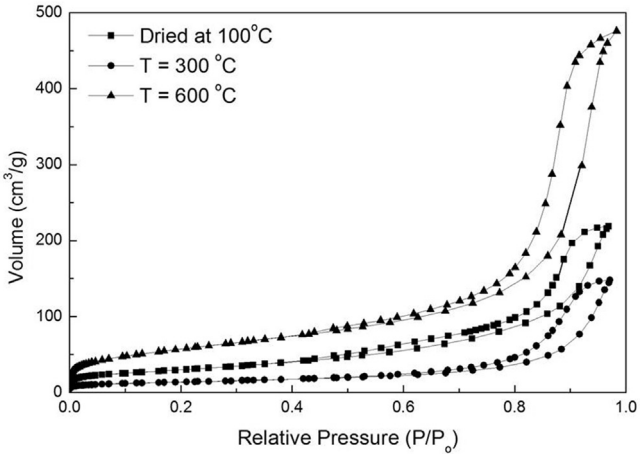

Fig. 8. N_2 adsorption/desorption isotherms of hydroxyapatite mixed with latex beads and calcined at different temperatures.

sample dried at 100 °C has a typical behavior of hydroxyapatite granules. Its surface area is 108.25 $m^2\ g^{-1}$. Part of the sample is not able to adsorb N_2 gas and the adsorption begins at P/Po close to 0.4. There is not change in adsorption behavior with heat treatment at 300 °C but a homogeneous decrease of the isotherm curve. Its surface area decreases to a lower value compared to dried sample (48.74 $m^2\ g^{-1}$) and the adsorption begins at P/Po close to 0.6. This trend can be associated to blocking of the sample by latex beads in the inner part of hydroxyapatite sample. It has not been inserted in the graph but the sample treated at 400 °C has a non porous behavior without any gas adsorption. After this temperature, an increase in gas adsorption is observed until 600 °C, when there is a complete removal of latex beads. However, the profile of isotherm adsorption curve has not changed as it can be seen and the adsorption returns to begins at P/Po close to 0.4 as it was observed for dried sample. This feature shows that the sample has the same pore shape but other routes have been opened for gas adsorption inside hydroxyapatite sample eliminating the blocking of the pores by aggregates. These new pores change the pore size distribution which cannot be considered more as a single distribution but there is contribution of inner pores close to spherical shell generated by latex bead remotion. The final result is the increase of adsorption capacity in terms of surface area (211.03 $m^2\ g^{-1}$) without changing the original morphology of hydroxyapatite particles.

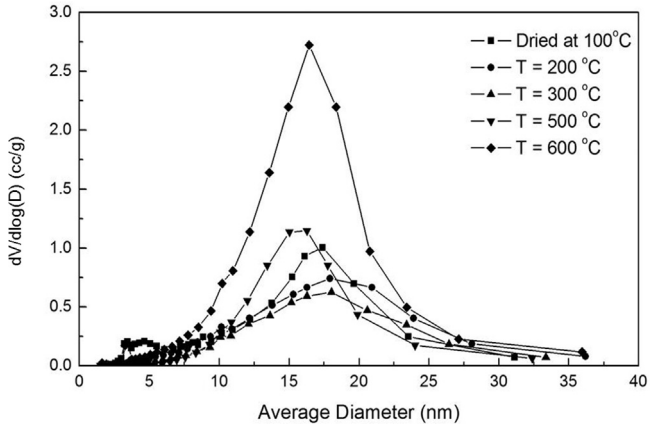

Fig. 9. Pore size distribution for hydroxyapatite mixed with latex beads and calcined at different temperatures.

Fig. 9 shows the changes in adsorption capacity of hydroxyapatite mixed with micrometric latex beads with the heat treatment temperature. There is a decrease in adsorption capacity from the dried sample until 300 °C. This feature can be associated with the incomplete removal of latex beads and densification of the sample, as observed in the TEM characterization (Fig. 5A). The pores are filled during the glass transition of the latex beads. Consequently, the mesopores are partially blocked, and the curve distribution shifts to higher pore diameter.

It is also observed that there are more available sites for gas adsorption because of an increase in pore volume for higher temperature. There is a broadening of the pore size distribution for the sample that was treated at 600 °C, which shows that the latex beads can modify the adsorption capacity of hydroxyapatite. In this method, molecule incorporation will be favored because there are more pores suitable for surface funcionalization after the remotion of latex beads. The pore size distribution is centered in the range of 15–20 nm, which are similar values to those found in literature [11].

The mean pore size during adsorption process was determined by BET method. This value for hydroxyapatite treated at 600 °C/1 h is 8.7 nm. The porosity degree of hydroxyapatite was also determined as 70% considering its bulk density as 3.10 g/cm^3 [50] and adsorption cumulative pore volume around 0.73 cm^3/g. This value is close to that value found for hydroxyapatite ceramic applied to bone tissue engineering (~75%) described by Yoshikawa et al. [51]. They adopted a foam gel technique which resulted in interconnected porous structure for hydroxyapatite with pore sizes estimated at 150 μm much more larger than that size scale of latex beads (~1.3 μm).

Fig. 10A shows the experimental SAXS data, the IFT fit and Fig. 10B the resulting volume distribution V(r). Interestingly, the main change in the SAXS profile (and consequently in the volume distribution function) happened for hydroxyapatite calcined at 400 °C/1 h. The volume distributions have two well-defined initial maxima and extend to large values of r. The first maximum is probably an artefact related to a constant background present in the system. However, the most pronounced maximum indicates a characteristic size that occupies the largest volume fraction in the system. Interestingly, up to 400 °C this value is around 40 Å. For 500 °C and 600 °C, there is a widening of this maximum and a shift to larger values (50–60 Å), indicating an increase of the characteristic distances within the system. The shape of this curve is typical of a system composed of pores and channels since the size of the channels can be quite large, inducing an increase in the size of the diameters in the distribution.

Surface area of the hydroxyapatite samples depends on the heat treatment temperature (Table 1). There is a decrease in surface area until 300 °C, and without gas adsorption by the sample, it calcined at 400 °C. The decrease of the adsorption capacity of this material can be associated to melting of latex beads covering hydroxyapatite particles as it was observed by TEM images (Fig. 5E and F). Above this temperature, the removal of latex beads begins in temperature range of 500–600 °C. These results are in agreement with the SEM characterization at Fig. 3. Therefore, the surface area significantly increases and more sites are available for gas adsorption after the complete combustion of latex bead. The surface area value for a heat-treated sample at 600 °C is close to that reported by Diaz et al. [52] for hydroxyapatite grown at biocompatible mesoporous ordered silica.

Fig. 11 displays different microscopy images for hydroxyapatite treated at 600 °C at two different magnifications in order to analyze how its morphology and topography at micrometric scale is. The overall structure is compact with some pores randomically distributed at external surface formed mainly by micrometic

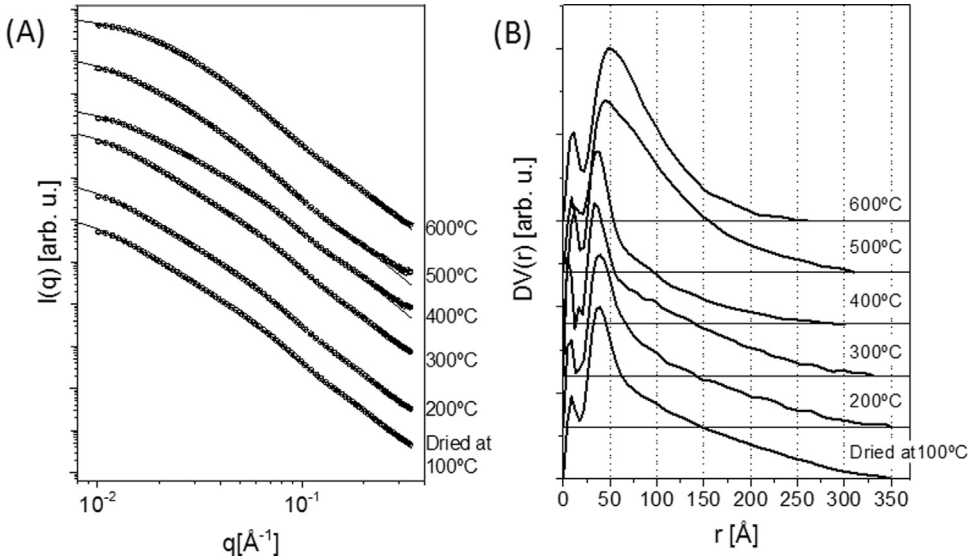

Fig. 10. SAXS results for calcined samples. (A) – Experimental SAXS data (symbols) and theoretical fits using IFT method (solid lines). (B) – Volume distribution function DV(r) obtained from the IFT method. In both cases the curves were shifted for clarity.

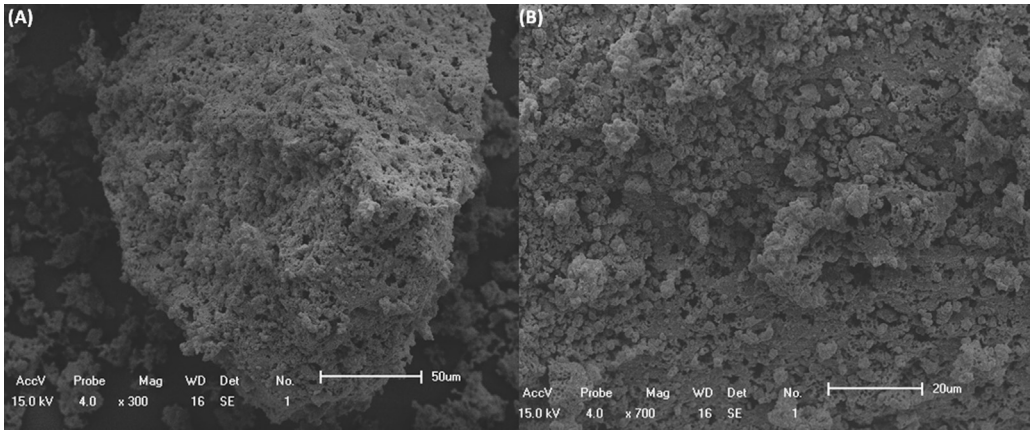

Fig. 11. SEM images of hydroxyapatite mixed with latex beads and calcined at 600 °C: (A) – micrometric cluster; (B) – general view of porous surface.

aggregates without any defined shape (Fig. 11A). It can be seen at more magnified view that the sample is not only covered by dense hydroxyapatite at external surface but there are channels introduced by latex beads soaked below hydroxyapatite aggregates (Fig. 11B). It is expected that these large channels contribute for more high surface area for this sample heat treated at 600 °C because they restrict aggregates growth during the synthesis process and they open new routes to integration of hydroxyapatite with living tissues.

The incorporation of latex beads into hydroxyapatite particles changes their surface area increasing the availability of new pores to incorporation of molecules. They can be a new route to cell growth and adsorption of drugs into living tissues. Fig. 12 gives an overview of the contribution of this new approach to build macroporous hydroxyapatite: (I) – Mix of latex beads and hydroxyapatite particles forming a nanacomposite stable until 200 °C; (II) – Melting of latex beads spreading along whole inorganic framework and isolating hydroxyapatite particles. This process happens at temperature range from 300 to 400 °C when pores are completely filled by latex beads resulting in strong decrease of surface area; (III) – Remotion of latex beads template generating an open structure at 600 °C. The main feature at the end of process is the increase of surface area due to broadening of the pore size distribution. (IV) – Hollow structures and a high surface area (>200 $m^2\ g^{-1}$) are important factors for drug release as it has been observed for hollow hierarchical porous hydroxyapatite with dimension of about 3 μm [53]. Other reports in the literature show that a polymer composite with hydroxyapatite can change their properties like density [54] or to be functionalized with carboxylic groups, which are able to bind to Ca^{2+} ions [55]; (V) – The presence of large porous embedded into macroporous hydroxyapatite scaffold can be able to mimic the structure and biological function of living tissues promoting adhesion, proliferation and differentiation in a similar way that observed for emulsion-templated polymers [56]. In this way, nanoscale hydroxyapatite generated in this work can be very useful for implants as it has been highlighted by Zhou et al. [57] for scaffold fabricated for different polymer matrices.

Fujishima et al. [2] reported the presence of three types of pores in hydroxyapatite templated by latex beads: mesopores, submicrometer-sized macropores of inverse opal structure and sponge-like larger macropores. Mesopores can be associated with the generation of nanoparticles by hydroxyapatite, and submicrometer sized is related to the original ordering of latex beads. The sponge-like larger macropores are related to thermal behavior of polystyrene particles. There is the melting of latex beads developing necks between hydroxyapatite nanoparticles. It is expected that our samples mainly have a mesoporous architecture surrounded by huge macropores. This feature is the main contribution of this synthesis route. Three points must be highlighted: i) latex beads are present in all stages of the synthesis; ii) latex beads are completely mixed to hydroxyapatite with no preferential ordering; and iii) melting process happens at a slow rate without disturbing the crystallization process of hydroxyapatite. The crystallites are isolated during the heat treatment, and they do not increase keeping its original size from amorphous sample. However, the slow latex removal induces an increase of mesopores along all samples causing an increase of the surface area. It is expected that this feature will play a vital role for application of this new material in biomaterials field because it results in an open porous surface constituted by a combination of huge pores and small hydroxyapatite crystallites. It will be necessary to analyze how to adjust this scale size of micrometric latex beads in scaffolds for tissue engineering because they have generally dimensions in the range from 10–100 μm. Other properties like osteoconductivity and mechanical strength will determine if this kind of hydroxyapatite will be better in terms of biocompatibility and biodegrability than those found in commercials scaffolds or drug release systems. Many other applications can be cited for hydroxyapatite outside biomaterials field due to discovery of new morphologies like microspheres, microcubes, microrods, nested bundles [58]. One of the predictable applications for hydroxyapatite synthesized in this work is nanofiltration. There has been already reported the removal of Pb^{2+} and fluoride ions by hydroxyapatite whose porous structure was determined by organic templates [59,60]. Therefore, other research directions may happen for a future application of hydroxyapatite described in this work. This feature will be bound mainly to the increase of its surface area after template removal.

4. Conclusion

Latex beads may be a good method to alter the surface properties of hydroxyapatite without modifying its crystalline structure. These beads change the distribution of hydroxyapatite particles by adding huge spherical macropores into the bulk of the biomaterial, which promotes an increase in surface area. The latex beads must be removed at temperatures higher than 500 °C to avoid blocking the hydroxyapatite pores because of the glass transition of the polymer. This new porous hydroxyapatite structure can reach a surface area higher than 200 $m^2\ g^{-1}$ and a porosity degree close to 70% after heat treatment at 600 °C/1 h. These features show that latex beads template can be a viable route to synthesize not only scaffolds or drug release systems but also other functional devices like nanofilters and catalyzers.

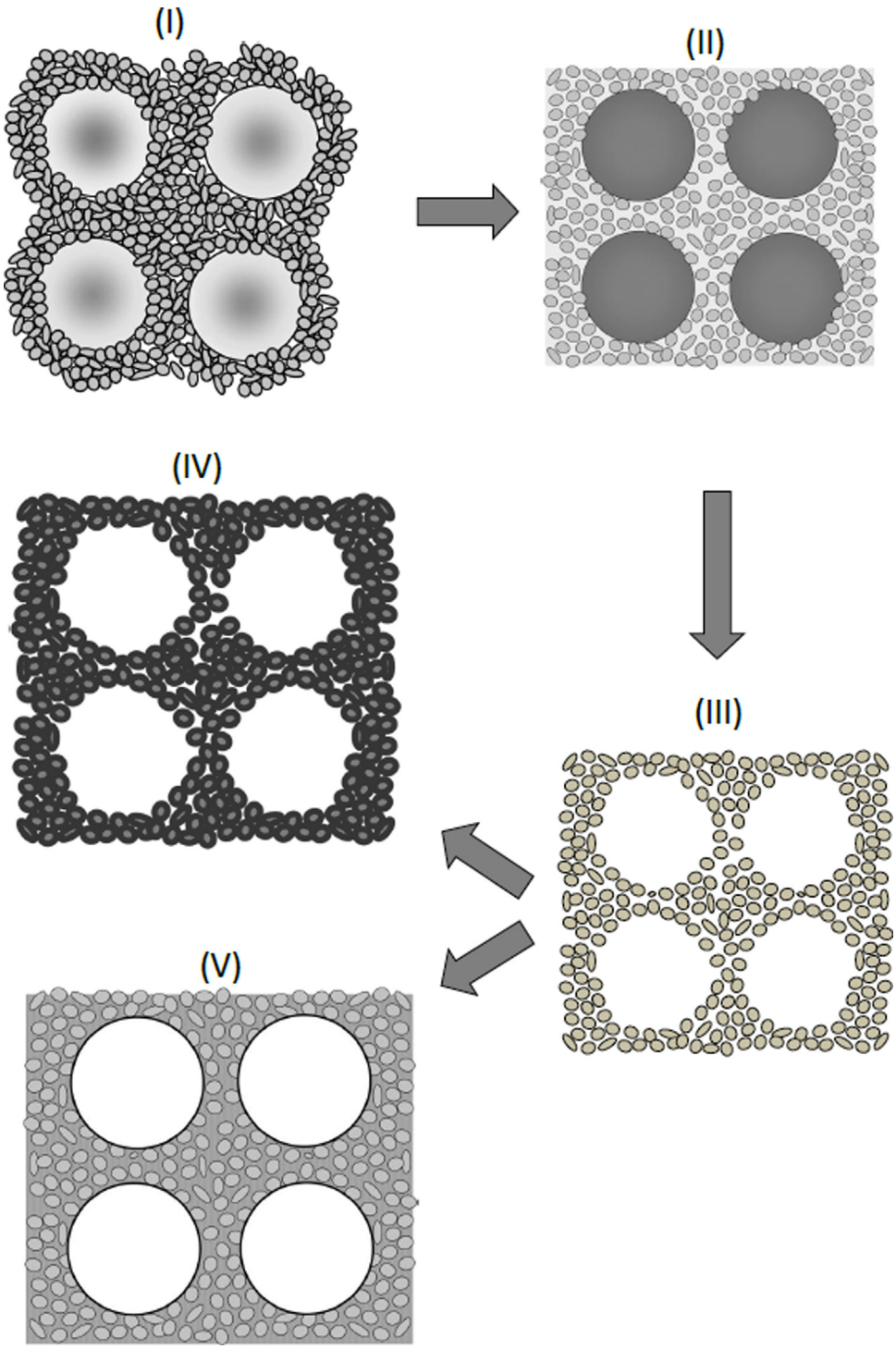

Fig. 12. Preparation steps and applications for macroporous hydroxyapatite: (I) – nanocomposite formation; (II) – expansion of latex beads into hydroxyapatite particles; (III) – remotion of latex beads template; (IV) – macroporous hydroxyapatite for drug delivery; (V) – application of macroporous hydroxyapatite for tissue engineering.

Acknowledgments

This work was supported by CAPES, Pró-equipamentos/PROCAD/PROCAD-NF, Pronex/FAPEAL, CNPq/MCT, CNPQ (Grant Number: 487978/2013-7/CNPq), PROMOB/CooperNano SE/AL and FINEP. The authors would like to acknowledge Dr. Celso Santilli from UNESP – Araraquara for the experimental support in the N_2 adsorption measurement.

References

[1] B.J. Melde, A. Stein, Periodic macroporous hydroxyapatite-containing calcium phosphates, Chem. Mater. 14 (2002) 3326–3331.
[2] M. Fujishima, Y. Okawa, K. Uchida, Hierarchical trimodal porous hydroxyapatite fabricated by colloidal crystal templating using single-size latex particles, J. Am. Ceram. Soc. 91 (2008) 3749–3752.
[3] K. Hwang, J. Song, B. Kang, Y. Park, Sol-gel derived hydroxyapatite films on alumina substrates, Surf. Coat. Technol. 123 (2000) 252–255.

[4] C.M. Lopatin, V. Pizziconi, T.L. Alford, T. Laursen, Hydroxyapatite powders and thin films prepared by a sol-gel technique, Thin Solid Films 326 (1998) 227–232.
[5] C. Li-yun, Z. Chuan-bo, H. Jian-feng, Influence of temperature, [Ca^{2+}], Ca/P ratio and ultrasonic power on the crystallinity and morphology of hydroxyapatite nanoparticles prepared with a novel ultrasonic precipitation method, Mater. Lett. 59 (2005) 1902–1906.
[6] M. Wei, A.J. Ruys, B.K. Milthorpe, C.C. Sorrell, Precipitation of hydroxyapatite nanoparticles: effects of precipitation method on electrophoretic deposition, J. Mater. Sci.-Mater. Med. 16 (2005) 319–324.
[7] W.J. Shih, M.-C. Wang, M.-H. Hon, Morphology and crystallinity of the nanosized hydroxyapatite synthesized by hydrolysis using cetyltrimethylammonium bromide (CTAB) as a surfactant, J. Cryst. Growth 275 (2005) e2339–e2344.
[8] W. Pon-On, S. Meejoo, I.M. Tang, Formation of hydroxyapatite crystallites using organic template of polyvinyl alcohol (PVA) and sodium dodecyl sulfate (SDS), Mater. Chem. Phys. 112 (2008) 453–460.
[9] J.H. Lee, I.T. Kim, R. Tannenbaum, M.L. Shofner, Synthesis of polymer-decorated hydroxyapatite nanoparticles with a dispersed copolymer template, J. Mater. Chem. 22 (2012) 11556–11560.
[10] Y.F. Zhao, J. Ma, Triblock co-polymer templating synthesis of mesostructured hydroxyapatite, Microporous Mesoporous Mater. 87 (2005) 110–117.
[11] A. Ethirajan, U. Ziener, K. Landfester, Surface-functionalized polymeric nanoparticles as templates for biomimetic mineralization of hydroxyapatite, Chem. Mater. 21 (2009) 2218–2225.
[12] A.A. Campbell, G.E. Fryxell, J.C. Linehan, G.L. Graff, Surface-induced mineralization: a new method for producing calcium phosphate coatings, J. Biomed. Mater. Res. 32 (1996) 111–118.
[13] P. Duheyne, J. Beight, J. Cuckler, B. Evans, S. Radin, Effect of calcium phosphate coating characteristics on early post-operative bone tissue ingrowth, Biomaterial 11 (1990) 531–540.
[14] M. Jie, L. Huiming, L. Xiaofeng, B. Chunhui, X. Di, Q. Fengyu, Synthesis of hierarchical porous bioactive glasses for bone tissue regeneration, Nanobiotechnol. IET 8 (2013) 216–221.
[15] F. Munarin, P. Petrini, R. Gentilini, R.S. Pillai, S. Dirè, M.C. Tanzi, V.M. Sglavo, Micro- and nano-hydroxyapatite as active reinforcement for soft Biocomposites, Int. J. Biol. Macromol. 72 (2015) 199–209.
[16] Z.-Y. Qiu, C.-S. Tao, H. Cui, C.-M. Wang, F.-Z. Cui, High-strength mineralized collagen artificial bone, Front. Mater. Sci. 8 (2014) 53–62.
[17] J. Chevalier, L. Gremillard, Ceramics for medical applications: a picture for the next 20 years, J. Eur. Ceram. Soc. 29 (2009) 1245–1255.
[18] A. Kuttor, M. Szaloki, T. Rente, F. Kerenyi, J. Bako, I. Fabian, I. Lazar, A. Jenei, C. Hegedus, Preparation and application of highly porous aerogel-based bioactive materials in dentistry, Front. Mater. Sci. 8 (2014) 46–52.
[19] S. Schachschal, A. Pich, H.J. Adler, Aqueous microgels for the growth of hydroxyapatite nanocrystals, Langmuir 24 (2008) 5129–5134.
[20] Z.A.C. Schnepp, R. Gonzalez-McQuire, S. Mann, Hybrid biocomposites based on calcium phosphate mineralization of self-assembled supramolecular hydrogels, Adv. Mater. 18 (2006) 1869–1872.
[21] S.H. Rhee, Y. Suetsugu, J. Tanaka, Biomimetic configurational arrays of hydroxyapatite nanocrystals on bio-organics, Biomaterial 22 (2001) 2843–2847.
[22] V.M. Rusu, C.H. Ng, M. Wilke, B. Tiersch, P. Fratzl, M.G. Peter, Size-controlled hydroxyapatite nanoparticles as self-organized organic-in organic composite materials, Biomaterial 26 (2005) 5414–5426.
[23] S. Fujii, M. Okada, T. Nishimura, T. Sugimoto, H. Maeda, H. Hamasaki, T. Furuzono, Y. Nakamura, Hydroxyapatite-coated poly(ϵ-caprolactone) microspheres fabricated via a pickering emulsion route: effect of fabrication parameters on diameter and chemical composition, Compos. Interface 20 (2013) 45–56.
[24] N.A. Kotov, Y. Liu, S. Wang, C. Cumming, M. Eghtedari, G. Vargas, M. Motamedi, J. Nichols, J. Cortiella, Inverted colloidal crystals as three-dimensional cell scaffolds, Langmuir 20 (2004) 7887–7892.
[25] C.A. Vacanti, L.J. Bonassar, An overview of tissue engineered bone, Clin. Orthop. 367 (1999) S375–S381.
[26] C.A. Vacanti, J.P. Vacanti, Bone and cartilage reconstruction with tissue engineering approaches, Otolaryngol. Clin. N. Am. 27 (1994) 263–276.
[27] R.A. Ayers, S.J. Simske, C.R. Nunes, L.M. Wolford, Long-term bone ingrowth and residual microhardness of porous block hydroxyapatite implants in humans, J. Oral Maxillofac. Surg. 56 (1998) 1297–1301.
[28] H. Yoshikawa, A. Myoui, Bone tissue engineering with porous hydroxyapatite ceramics, J. Artif. Organs 8 (2005) 131–136.
[29] C. Du, F.Z. Cui, X.D. Zhu, K. de Groot, Three-dimensional nano-HAp/collagen matrix loading with osteogenic cells in organ culture, J. Biomed. Mater. Res. 44 (1999) 407–415.
[30] G. Wei, G.J. Pettway, L.K. McCauley, P.X. Ma, The release profiles and bioactivity of parathyroid hormone from poly(lactic-*co*-glycolic acid) microspheres, Biomaterial 25 (2004) 345–352.
[31] M.P. Ginebra, T. Traykova, J.A. Planell, Calcium phosphate cements as bone drug delivery systems: a review, J. Control. Release 113 (2006) 102–110.
[32] L. Kong, Y. Gao, W. Cao, Y. Gong, N. Zhao, X. Zhang, Preparation and characterization of nano-hydroxyapatite/chitosan composite scaffolds, J. Biomed. Mater. Res. 75A (2005) 275–282.
[33] W. Li, L. Yubao, Z. Yi, Z. Li, Z. Qin, C. Lin, J. Hong, Porous bioactive scaffold of aliphatic polyurethane and hydroxyapatite for tissue regeneration, Biomed. Mater. 4 (2009) 025003.
[34] G. Wei, P.X. Ma, Structure and properties of nano-hydroxyapatite/polymer composite scaffolds for bone tissue engineering, Biomaterial 25 (2004) 4749–4757.
[35] Y.-C. Fu, H. Nie, M.-L. Ho, C.-K. Wang, C.-H. Wang, Optimized bone regeneration based on sustained release from three-dimensional fibrous PLGA/HAp composite scaffolds loaded with BMP-2, Biotechnol. Bioeng. 99 (2008) 996–1006.
[36] J.S. Son, M. Appleford, J.L. Ong, J.C. Wenke, J.M. Kim, S.H. Choi, D.S. Oh, Porous hydroxyapatite scaffold with three-dimensional localized drug delivery system using biodegradable microspheres, J. Control. Release 153 (2011) 133–140.
[37] T.P. Richardson, M.C. Peters, A.B. Ennett, D.J. Mooney, Polymeric system for dual growth factor delivery, Nat. Biotechnol 19 (2001) 1029–1034.
[38] X.Q. Zhang, J. Intra, A.K. Salem, Comparative study of poly(lactic-*co*-glycolic acid)-poly ethyleneimine-plasmid DNA microparticles prepared using double emulsion methods, J. Microencapsul. 25 (2008) 1–12.
[39] S.H. Choi, T.G. Park, G-CSF loaded biodegradable PLGA nanoparticles prepared by a single oil-in-water emulsion method, Int. J. Pharm. 311 (2006) 223–228.
[40] S.E. Bae, J.S. Son, K. Park, D.K. Han, Fabrication of covered porous PLGA microspheres using hydrogen peroxide for controlled drug delivery and regenerative medicine, J. Control. Release 133 (2009) 37–43.
[41] H.K. Kim, H.J. Chung, T.G. Park, Biodegradable polymeric microspheres with "open/closed" pores for sustained release of human growth hormone, J. Control. Release 112 (2006) 167–174.
[42] A.L. Patterson, The Scherrer formula for X-ray particle size determination, Phys. Rev. 56 (1939) 978–982.
[43] A.V. Semenyuk, D.I. Svergun, GNOM—a program package for small-angle scattering data processing, J. Appl. Cryst. 24 (1991) 537–540.
[44] S.J. Gregg, K.S.W. Sing, Adsorption, Surface Area and Porosity, Academic Press, London, 1967.
[45] M. Kruk, M. Jaroniec, Gas adsorption characterization of ordered organic-inorganic nanocomposite materials, Chem. Mater. 13 (2001) 3169–3183.
[46] K.S.W. Sing, D.H. Everett, R.A.W. Haul, L. Moscou, R.A. Pierotti, J. Rouquerol, T. Siemieniewska, Reporting physisorption data for gas/solid systems with special reference to the determination of surface area and porosity, Pure Appl. Chem. 57 (1985) 603–619.
[47] P.B. Aielo, F.A. Borges, K.M. Romeira, M.C.R. Miranda, L.B.D. Arruda, P.N.L. Filho, B.D.C. Drago, R.D. Herculano, Evaluation of sodium diclofenac release using natural rubber latex as carrier, Mater. Res. 17 (2014) 146–152.
[48] R.M. Wilson, J.C. Elliott, S.E.P. Dowker, Rietveld refinement of the crystallographic structure of human dental enamel apatites, Am. Mineral. 84 (1999) 1406–1414.
[49] G.F. Scalera, K.P. Sanosh, A. Sannino, A. Licciulli, Influence of the calcination temperature on morphological and mechanical properties of highly porous hydroxyapatite scaffolds, Ceram. Int. 39 (2013) 4839–4846.
[50] H.M. Rootare, R.G. Craig, Characterization of the compaction and sintering of hydroxyapatite powders by mercury porosimetry, Powder Technol. 9 (1974) 199–211.
[51] H. Yoshikawa, N. Tamai, T. Murase, A. Myoui, Interconnected porous hydroxyapatite ceramics for bone tissue engineering, J. R. Soc. Interface 6 (2009) S341–S348.
[52] A. Diaz, T. Lopez, J. Manjarrez, E. Basaldella, J.M. Martinez-Blanes, J.A. Odriozola, Growth of hydroxyapatite in a biocompatible mesoporous ordered silica, Acta Biomater. 2 (2006) 173–179.
[53] H. Yang, L. Hao, N. Zhao, C. Du, Y. Wang, Hierarchical porous hydroxyapatite microsphere as drug delivery carrier, CrystEngComm 15 (2013) 5760–5763.
[54] D. Rosu, C.N. Cascaval, L. Rosu, Synthesis and characterization of some composites with bioactive properties on the basis of vinyl ester resins, e-Polymers (2008) 1–10.
[55] M. Hood, M. Mari, R. Muñoz-Espí, Synthetic strategies in the preparation of polymer/inorganic hybrid nanoparticles, Materials 7 (2014) 4057.
[56] H. Zhang, A.I. Cooper, Synthesis and applications of emulsion-templated porous materials, Soft Matter 1 (2005) 107–113.
[57] H. Zhou, J. Lee, Nanoscale hydroxyapatite particles for bone tissue engineering, Acta Biomater. 7 (2011) 2769–2781.
[58] I.R. Mary, S. Sonia, S. Viji, D. Mangalaraj, C. Viswanathan, N. Ponpandian, Novel multiform morphologies of hydroxyapatite: synthesis and growth mechanism, Appl. Surf. Sci. 361 (2016) 25–32.
[59] M.S. Fernando, R.M. de Silva, K.M.N. de Silva, Synthesis, characterization, and application of hydroxyapatite and nanocomposite of hydroxyapatite with granular activated carbon for the removal of Pb^{2+} from aqueous solutions, Appl. Surf. Sci. 351 (2015) 95–103.
[60] Z. Ruan, Y. Tian, J. Ruan, G. Cui, K. Iqbal, A. Iqbal, H. Ye, Z. Yang, S. Yan, Synthesis of hydroxyapatite/multi-walled carbon nanotubes for the removal of fluoride ions from solution, Appl. Surf. Sci. 412 (2017) 578–590.